Synsint Research Group

Available online at www.synsint.com

Synthesis and Sintering

ISSN 2564-0186 (Print), **ISSN** 2564-0194 (Online)

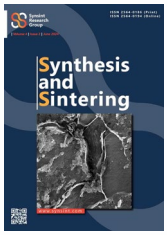

Research article

Comparing the effects of different sintering aids on spark plasma sintering of SiC ceramics

A. Faeghinia

Ceramics Department, Materials and Energy Research Center (MERC), P.O. Box 31779-83634, Karaj, Iran

ABSTRACT

In the present work, to improve the mechanical properties of silicon carbide different sintering aids were used. 2.5 wt% B_4C, 2.5 wt% AlN, and TiC in the range of 5 to 7 wt% were selected to manufacture the SiC-based sample via spark plasma sintering at 1700 °C. The results show that the use of 2.5 wt% B_4C-2.5 wt% AlN additives increases the strength (1206 MPa) of the composite through the compressive stress created in the grain boundaries and decreases its fracture toughness (5.13 MPa.$m^{1/2}$). But in the case of TiC-doped SiC, the toughness (7.09 MPa.$m^{1/2}$) and density (3.18 g/cm^3) of the sample increases compared to the pure SiC sample.

KEYWORDS

Silicon carbide
Sintering aid
Spark plasma sintering
Mechanical properties

OPEN ACCESS

1. Introduction

As a member of high-temperature structural ceramics silicon carbide (SiC) is broadly utilized in different fields like thermal engineering, mechanical engineering, and aerospace, owing to its outstanding structural features such as high melting temperature, high hardness, superior chemical stability, and considerable resistance to oxidation, wear, and corrosion [1–3].

However, the sintering temperature of monolithic SiC ceramics typically exceeds 2000 °C due to the strong covalent bonding characteristics of SiC, which results in a coarser microstructure and deterioration of mechanical properties [4, 5].

The enhancement of fracture toughness in silicon carbide ceramics has been widely recognized by incorporating of borides and metal carbides as reinforcing phases. To further enhance the properties of SiC, secondary phases such as titanium carbide (TiC), boron carbide (B_4C), and titanium diboride (TiB_2) have also been employed in the fabrication of SiC-based materials [6, 7]. Moreover, by utilizing temperatures exceeding 2200 °C, the prevalence of covalent bonds and the low self-diffusion characteristic permit the complete sintering of SiC to attain high density without the use of sintering aids. Notably, the achievement of nearly 100% theoretical density in pure SiC solely relies on hot pressing at 2500 °C and 50 MPa [7]. Extensive endeavors have been undertaken to seek suitable sintering aids for solid-state or liquid-phase sintering of SiC. Prochazka and Scanlan [8] successfully achieved a density of 96.4% in SiC through solid-state sintering with the inclusion of B_4C, albeit necessitating temperatures beyond 2100 °C. Other investigations have demonstrated that additives such as B and C contribute to densification, facilitate the β to α transformation, and augment the presence of plate-like α-SiC within the β-SiC matrix. Nevertheless, at temperatures surpassing 2000 °C, challenges including grain growth emerge. Thus, it is intriguing to explore alternative additives that can suppress the β to α transformation and enhance the mechanical properties [9].

The addition of SiO_2 in SiC ceramics can inhibit the transformation of β-SiC to α-SiC by preventing the volume increase of β-SiC particles during sintering. The SiO_2 layer also partially impedes grain growth, affecting the overall phase transformation of SiC [10].

Efforts have been made to impede the transformation of the α phase to the β phase, employing techniques such as mechanical alloying and prolonged ball milling. These methods aim to induce disorder in the carbide phase alongside the aluminum nitride phase [11].

Phase stability in the SiC-AlN system is observed between 2100 °C and 2300 °C. The β phase remains stable with AlN concentrations from

* Corresponding author. *E-mail address:* a.faeghinia@merc.ac.ir (A. Faeghinia)

Received 1 November 2023; Received in revised form 16 April 2024; Accepted 18 April 2024.

https://doi.org/10.53063/synsint.2024.42187

about 2 mol% up to 14 mol%, while the α phase is stable at AlN concentrations above 23 mol% [12]. Another role of carbon was to react with the SiO_2 layer on the surfaces of the SiC particles, eliminating it and forming secondary in-situ SiC. Additionally, the diffusion of boron into the SiC lattice decreased the energy of grain boundaries [13].

Near-fully dense SiC was successfully fabricated and a relative density of 97.5% was obtained for pure SiC using SPS at 1950 °C with 100 MPa pressure by Maître et al. [14]. By using 0.86 wt% carbon and 3.1 wt% boron, they were able to further increase the density to 98.8%. The SPS of SiC with Al_2O_3–Y_2O_3 additives under 30 MPa pressure for 5 min holding time at 1800 °C has been reported by Tamari et al. [15]. The introduction of B_4C and Al_4C_3 into the SiC leads to achieving fully dense samples using a spark plasma sintering process at 1600 °C under 47 Mpa for holding times ranging from 2 to 5 min [16].

Alliegro et al. [17] investigated the impact of aluminum on the densification of SiC and discovered that adding 1 wt% of aluminum increased the SiC density to 98%. In contrast, Stutz et al. [18] found different results, achieving a maximum density of 87% for β-SiC by adding 2 wt% carbon and 1 wt% aluminum. Investigation of the sinterability of α-SiC with C and B_4C additives showed that the inclusion of 1 wt% C and 0.5 wt% B_4C increased the SiC density to 99% at 2050 °C [19].

The primary objective of this study is to elucidate the role of specific sintering aid additives-aluminum nitride (AlN), titanium carbide (TiC), and boron carbide (B_4C)-in the spark plasma sintering of silicon carbide. A comprehensive investigation was conducted to explore how these additives affect the densification process, microstructural evolution, and mechanical properties of the sintered SiC. By understanding the impact of each additive on the sintering mechanism and final material characteristics, this research aims to refine the selection and optimization of sintering aids for SPS of SiC. The ultimate goal is to enhance its applicability in high-performance engineering applications where exceptional material strength, toughness, and hardness are essential.

2. Experimental procedures

2.1. Materials and procedure

For the fabrication of ceramic composite specimens, the first step involved weighing silicon carbide (Parsian Nano Fanavar, <5 µm, ≥99%), titanium carbides (CAS No. 12070-08-5, <5 µm, ≥99%), aluminum nitride (CAS No. 24304-00-5, <6 µm, ≥98%), and boron carbide (CAS No. 12069-32-8, <10 µm, 98%) powders in various weight ratios as specified in Table 1. The percentage by weight was such that, for example, 2.5% of the total weight of the composite belonged to the additive.

Table 1. The amount (wt%) of additives used in the sintered samples.

	TiC	SiC	AlN	B_4C
H	4	94	0	2
O	0	100	0	0
F	0	95	2.5	2.5
U	7	93	0	0

These weighted powders were then mixed into ethanol. Subsequently, a high-energy planetary ball milling device was utilized to homogenize and mix the raw materials. The obtained slurry of the raw materials, along with silicon carbide balls, was placed in a wear-resistant Teflon container, and the milling process was conducted for 24 h. After mixing, the slurry was poured into a plaster mold and dried at 80 °C for 24 h to evaporate all the ethanol from the powder mixture. Then, the powder was ground using a ceramic mortar and subsequently sieved through a 200-mesh sieve to reduce agglomeration.

In the next step, the crushed powder mixtures were subjected to a temperature of 1100 °C for 1 h in a resistance furnace. This step aimed to decompose and eliminate any residual ethanol within the material structure.

After calcination, the samples proceeded to the sintering stage. All the composite samples were placed in a graphite mold and crucible. Initially, they were heated to a temperature of 980 °C for 15 min, followed by sintering at 1700 °C using the spark plasma sintering furnace (20 T-10, China). This process involved a heating rate of 100 °C/min and an applied pressure of 40 MPa at the maximum temperature.

The density and porosity of the samples were calculated according to the ASTM C373 standard using the Archimedes principle. The identification and analysis of crystalline phases were performed using an X-ray diffractometer (XRD) (Philips PW3710, Germany). The phase identification was done based on the corresponding phase PDF cards and using the X'Pert HighScore Plus (version 3.0) software. XRD test was conducted in the 2θ angle range of 10 to 80 degrees, using Cu Kα radiation with a wavelength of 1.5406 Å, voltage of 20 kV, and current intensity of 30 mA.

The flexural strength test was performed according to the ASTM C1161-13 standard using a compression strength device (Santam STM-20). Although the device reports flexural strength after conducting the test, for increased reliability and considering the limited number of samples, the three-point strength was calculated using Eq. 1:

$$\sigma = 3FL/2bd^2 \quad (1)$$

where σ represents the flexural or three-point strength in MPa, F is the maximum force applied at the moment of sample failure in N, L is the distance between the two supports under compression in mm, b is the width of the sample in mm, and d is the height of the sample in mm. Hardness testing was performed using a hardness tester (KM2/01–92123, Koopa Pazhoohesh, Iran). For hardness measurement, the prepared specimens were cold-mounted. The mounted specimens were then ground and polished, followed by hardness testing. For each specimen, measurements were taken at least 3 times from different locations at a specified distance from the previous measurements, and the average values were reported. In this method, the hardness values of the samples were calculated using Eq. 2. In this equation, H_v represents the Vickers hardness in MPa, F is the applied load in K_{gf}, and d is the average diagonal length in mm.

$$H_v = 1.854\ F/d^2 \quad (2)$$

Furthermore, in this method, the fracture toughness of the samples was measured using the Eq. 3 [20].

$$k_{IC} = 0.16\left(\frac{c}{a}\right)^{-1.5}\left(H_v a^{1/2}\right) \quad (3)$$

In which k_{IC} represents the fracture toughness, H_v is the Vickers hardness, C is the average length of the created cracks at the Vickers indentation tip, and a is half the length of the indentation diagonal.

3. Results and discussion

3.1. Phase evaluation

Fig. 1 depicts the phase evaluations of the obtained 4 SPSed samples. As observed, sample O exhibits both hexagonal and rhombohedral structures of SiC, indicating the transformation of the alpha to beta phase. The sintering process plays a crucial role in this transformation, as reported by various studies. The sintering conditions, atmosphere, and additives can influence this transformation [21, 22]. However, in other samples (H, F, U), especially sample U, the dominant phase is rhombohedral, which is influenced by the presence of 7 wt% of titanium carbide. Therefore, this carbide phase as a sintering aid plays a critical role in the formation of the rhombohedral phase. In samples F and H, both cubic and rhombohedral forms are present. Considering the different surface properties of rhombohedral and hexagonal in terms of hardness [23], different behavior is expected. The hexagonal phase terminates at carbon, while the rhombohedral phase terminates at silicon [24].

The hardness properties of various SiC polytypes are different owing to their distinct structures. The hexagonal form of SiC is incredibly hard, with bonds oriented in specific directions that surpass even diamond in hardness [25]. Rhombohedral polytypes such as 15R-SiC are also noteworthy, although they are less prevalent compared to hexagonal forms [26]. In contrast, the cubic form of SiC is known for its strong chemical and mechanical stability, providing resistance to elevated radiation and temperatures [27]. The hexagonal and rhombohedral polytypes exhibit anisotropic behavior due to their sixfold symmetry axis, which affects their physical characteristics [28]. Thus, while hexagonal SiC is notable for its superhardness, cubic SiC gets attention because of its stability and resistance to harsh conditions.

As can be seen, both samples O and F have rhombohedral silicon carbide phases, while sample F also contains aluminum boride phases. On the other hand, both samples H and U contain the titanium carbide phase, but sample U has a higher percentage (over 5 wt%), as indicated by the characterization. This phase is also associated with the silicon carbide phase. However, two additional peaks are present in sample F.

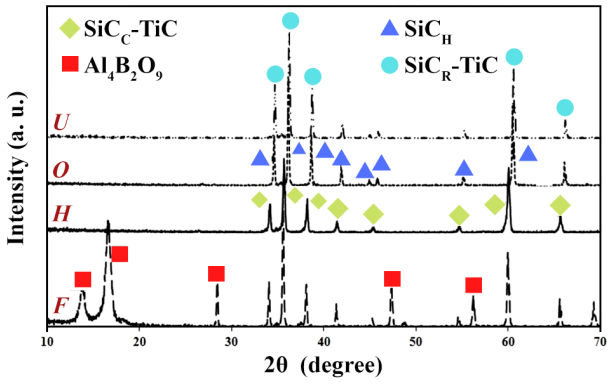

Fig. 1. Phase evaluation of the SiC samples sintered by SPS.

Notably, the addition of 7 wt% titanium carbide (TiC) induced a significant cubic to rhombohedral phase transformation in SiC. This transformation is evidenced by shifts in the position of the peaks and the appearance of new diffraction peaks corresponding to rhombohedral lattice planes. This evolution shows a significant effect of TiC on the crystal structure of SiC, which is probably related to lattice stress and distortion caused by TiC particles in the SiC matrix. Conversely, specimens augmented with aluminum nitride (AlN) and boron carbide (B_4C) demonstrated XRD patterns that suggested the stabilization of the SiC cubic structure. Identifiable peaks associated with cubic SiC remained prominent without shifts or the appearance of rhombohedral-associated peaks, underscoring the modulatory role of AlN and B_4C in preserving the integrity of the cubic crystalline framework. This retention of cubic structure signifies that incorporation of AlN and B_4C may effectively dampen the cubic to rhombohedral transformation, thereby manifesting a cardinal influence on the final mechanical properties of the sintered material.

3.2. Microstructure and mechanical properties

Fig. 2 shows the SEM images captured in secondary electron mode from the polished surfaces along with EDS analysis. It can be seen from Fig. 2 that by changing the type of additives, the grain size and porosity change.

Fig. 3 displays another SEM micrograph captured in back-scattered electron mode from the polished surface of the as-SPSed samples. Addition of additives has let to formation of new phases in the microstructures. The formation of new secondary phases not only can affect microstructure and densification, but also it has led to improvement of mechanical properties such as compressive strength showing in Table 2.

By comparing two identical samples sintered at a specific temperature, sample O (Figs. 2b and 3b) and sample F containing AlN and B_4C additives (Figs. 2c and 3c), it can be understood that addition of AlN and B_4C has played an effective role in increasing the compressive strength (Table 2). In addition to the strengthening mechanism through reinforcing particles, the mechanism of grain size reduction can also be mentioned [29].

In other words, by increasing the volume fraction of reinforcement particles, the grain size of the matrix phase decreases [30]. In the present study, by adding 2.5 wt% of AlN and B_4C to SiC particles, the grain size of SiC particles has decreased according to the Zener equation (Eq. 4):

$$Z = 4r/3f \quad (4)$$

where Z represents the size of the matrix grains, f is the volume fraction of the secondary phase, and r is the radius of the secondary particles.

In sample U, the addition of TiC and SiC particles on one hand induces residual stresses within the composite structure. These stresses transfer compressive residual stress to the grain boundaries, leading to enhanced fracture toughness and strength [31]. On the other hand, they act as a pinning agent and prevent their movement by being in the grain boundaries and preventing excessive grain growth. They also protect grain boundaries, which prevent crack propagation along them [32].

The application of the SPS method in the present study effectively resolves the agglomeration problem of SiC particles. This results in a strong bond between the SiC and TiC particles (samples H and U in

Table 2. The mechanical properties (hardness, toughness, bending and compressive strengths, and densities) of sintered samples.

Sample code	Compressive strength (MPa)	Bending strength (MPa)	Density (g/cm^3)	k_{IC} (MPa.m$^{1/2}$)	Microhardness (kgf.mm^{-2})
O	879	176.7	3.15	5.81	2968
H	890	186.7	3.16	6.57	2700
F	1206	157.9	3.08	5.13	2641
U	1175	144.5	3.18	7.09	2954

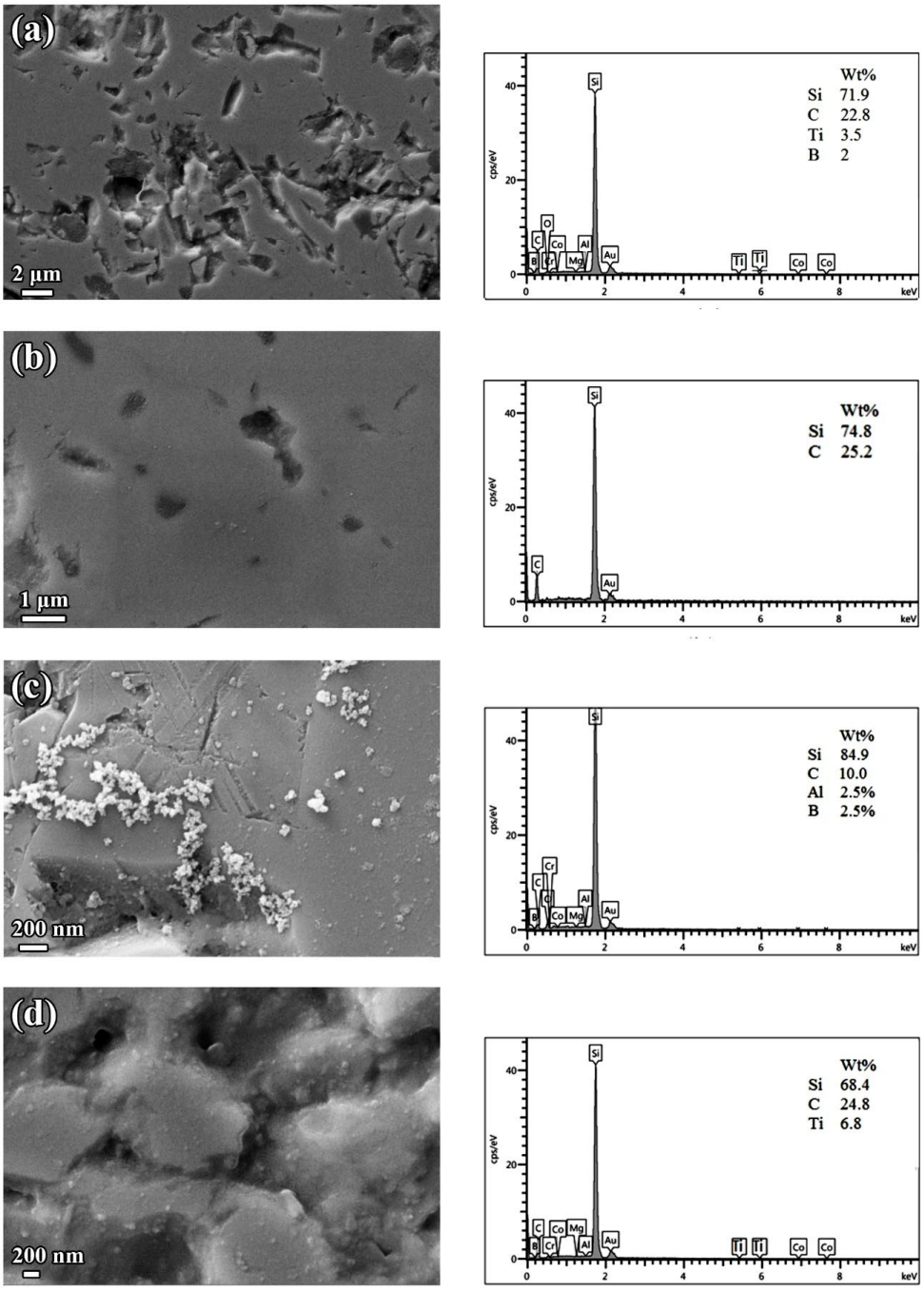

Fig. 2. The SEM micrographs of SPSed SiC with additives: a) sample H with 2000 × magnification, b) sample O with 1000 × magnification, c) sample F with 20000 × magnification, and d) sample U.

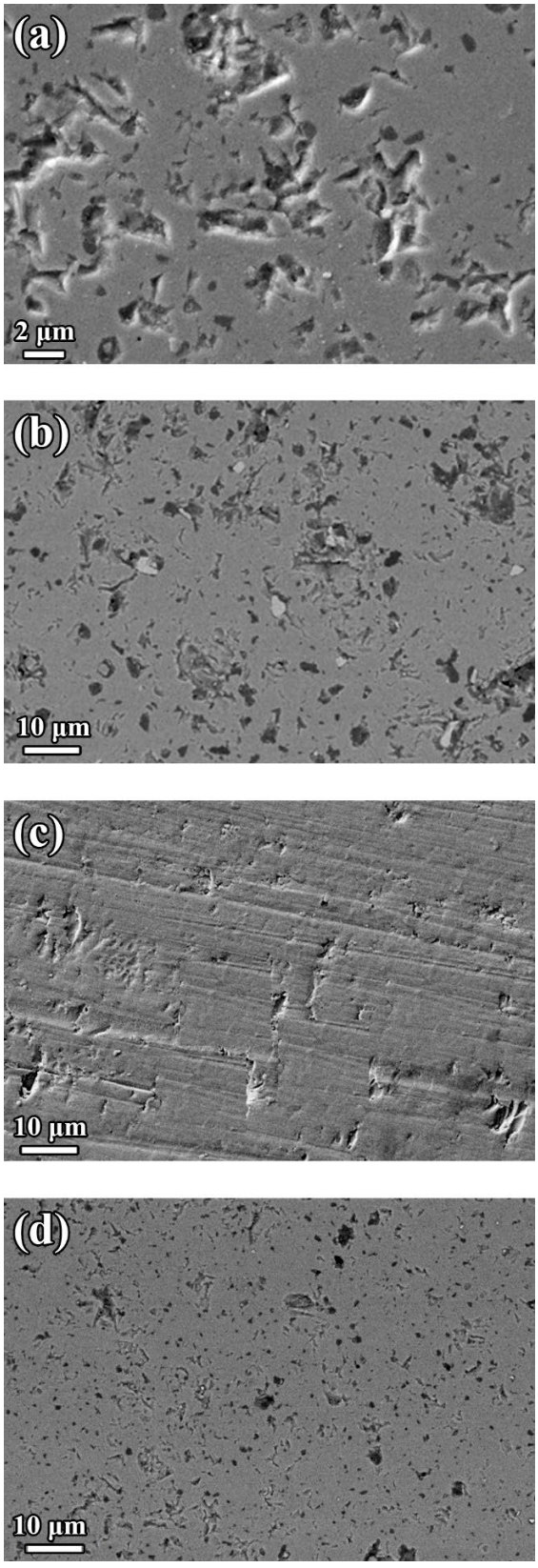

Fig. 3. The SEM micrographs of SPSed SiC with additives: a) sample H, b) sample F, c) sample O, and d) sample U with different magnification.

Fig. 3), encouraging better particle dispersion and promoting the overall structural integrity of the composite material. Consequently, the uniform distribution of TiC within the SiC matrix contributes to enhanced mechanical properties and performance of the sintered material.

The strong bonding and cohesive interface between the reinforcing particles and the matrix phase ultimately lead to a significant increase in the bending strength of the SPS-sintered composite samples. A proper charge transfer from the TiC matrix to the SiC reinforcement requires a suitable and strong bond at the interface [6]. Therefore, the bond between the reinforcing particles and the matrix directly affects mechanical properties such as flexural strength. With an increase in uniaxial pressure during the SPS process, the quality of the interface improves, and the bonding between SiC and AlN particles in sample F is enhanced. On the other hand, applying pressure during the sintering process reduces the porosity at the interface, resulting in an increase in the density and the compressive strength of the composite. These findings are in complete agreement with the other researchers' findings [33].

The SEM images revealed distinct differences in grain size, boundary formation, and porosity among samples with altered additive compositions. In the specimens doped with titanium carbide, a noticeable reduction in grain size was observed, which suggests that TiC acts as an inhibitor of grain growth during the sintering process. Conversely, the incorporation of aluminum nitride appeared to preserve the integrity of the grain boundaries, leading to a more homogenous microstructure with minimal porosity. The samples containing boron carbide exhibited a denser microstructure with a reduction in intergranular space, indicating an effective sintering aid contribution to the reduction of porosity. Samples with higher amounts of B_4C showed more uniform grain distribution, which is creatable with the enhanced compressive strength measurements discovered in mechanical testing. This comprehensive SEM analysis provides a linkage between the observed mechanical properties and the microstructural characteristics imparted by the different sintering aid additives.

In examining the densification behavior of SiC ceramics with various sintering aid additives, the measured density and porosity values serve as critical indicators of the effectiveness of the SPS process influenced by these additives. The Archimedes method provided quantitative data on these metrics shown in Table 2, revealing distinct correlations between additive content and sintered body characteristics. Particularly noteworthy was that SiC samples with AlN displayed moderately enhanced densities compared to pure SiC, which can be attributed to the stabilization effect of AlN on the SiC structure. However, the most eminent enhancement in density was observed in TiC-doped SiC samples. The addition of TiC significantly reduced porosity and increased the density, bringing it close to the theoretical maximum for SiC.

Conversely, the incorporation of B_4C resulted in a slight decrease in density. This could be due to the formation of B_4C-related boundary phases, which may inhibit the densification process or increase the presence of residual porosity. Sample U, containing 7 wt% TiC, showed superior densification with minimal porosity, suggesting that the TiC phase significantly contributes to the sintering process. This indicates that there is an optimal concentration of TiC that maximizes densification. The findings suggest a delicate balance between the

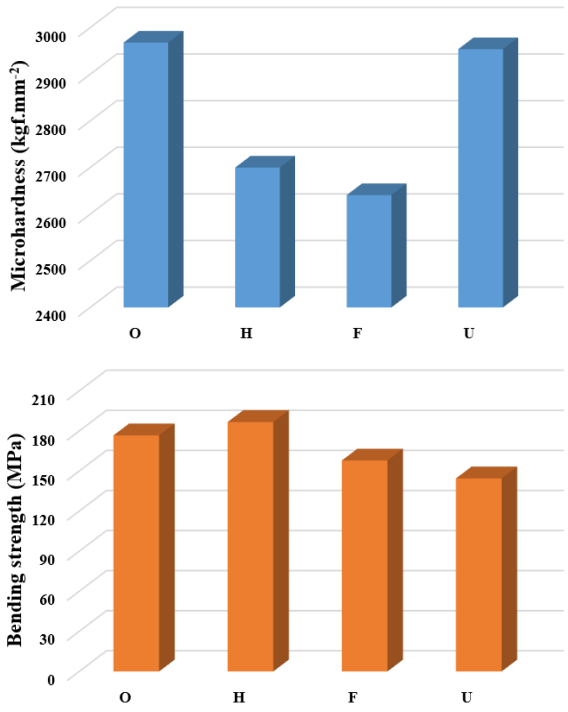

Fig. 4. The measured hardness and bending strength.

beneficial effects of additives in promoting densification and their potential to introduce secondary phases that impede full densification.

The results of hardness and strength measurement of the as-sintered samples are presented in Fig. 4. The highest hardness value, 2968 H_v equivalent to 61.29 GPa was obtained in sample O, indicating high densification and advancement of the sintering mechanism. This is attributed to the formation of beta particles and the presence of the hexagonal form of SiC during the sintering process. Additionally, the phase composition and morphology are other factors affecting the hardness. Due to the short sintering time of the plasma sintering method, it is possible to control grain growth and attain a narrower grain size distribution, thereby resulting in increased hardness. The application of pressure in this process improves densification and eliminates porosity.

The lowest hardness value, 2641 H_v equivalent to 26 GPa, was observed in sample F, while sample H exhibited higher hardness. According to the XRD results, it was observed that samples with a higher percentage of the TiC phase have higher hardness compared to samples with a higher percentage of other carbide and nitride phases. This is consistent with the reported results, which show that aluminum diffuses more than the boride phase in the SiC structure and leads to a significant change in their hardness [34]. Although elongation of SiC grains contributes to increased fracture toughness, (Figs. 2 and 4) their presence also leads to increased scatter and reduced strength [35].

One of the methods to improve the strength and fracture toughness of SiC is reinforcement with particles possessing different elastic and thermal properties, such as TiC [36] and TiB_2 [24]. It is believed that the differences in elastic, thermal, and fracture properties between the reinforcements and the SiC matrix activate some of the conventional strengthening mechanisms in these composites. For example, the higher thermal expansion coefficient of TiC ($\alpha = 7.7 \times 10^{-6}$ °C) [37, 38], compared to the SiC matrix ($\alpha = 4.5 \times 10^{-6}$ °C) [37, 39], creates

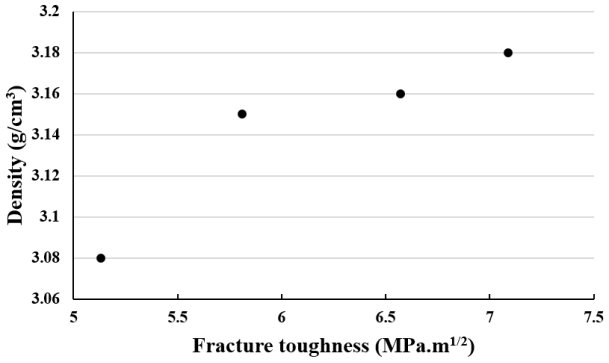

Fig. 5. The fracture toughness vs. density.

residual compressive stress around the TiC particles during cooling from the fabrication temperature [40, 41].

Fig. 5 demonstrates the variation of density versus fracture toughness. The compressive stress interacts with tensile stress at the crack tip, resulting in the creation of a new relaxed stress at the crack tip and increased fracture toughness of the composite [32]. In addition to the strengthening effect, the presence of reinforcement particles can also suppress the growth of SiC grains, which typically leads to improved strength [6]. Therefore, sample U has higher fracture toughness and density compared to other samples due to its 7 wt% TiC content.

The bending strengths, densities, and toughness values of sintered samples all together are shown in Fig. 6. As can be seen, sample H has the lowest fracture toughness among all samples but has the highest bending strength. This can be attributed to the elongated crystal shape and the increased interface with the reinforcement, as well as the hexagonal form of SiC. However, sample U has a rhombohedral structure.

Hardness testing results indicated that while every additive introduced led to a decrease in hardness compared to the pure SiC sample, the amplification of the TiC phase at 7 wt% contributed to an increase in hardness, highlighting the role of TiC in enhancing the material's resistance to plastic deformation.

According to Table 2, Compressive strength results showed a significant increase with the incorporation of B_4C, suggesting that the presence of B_4C at the grain boundaries effectively impedes dislocation movement, thereby enhancing the compressive load-bearing capabilities of the sintered composite. Toughness measurements showed a remarkable increase in samples with 7 wt% TiC, highlighting the ability of TiC to inhibit crack propagation and increase energy absorption before failure. These important deviations in mechanical behavior emphasize the obvious influence that sintering aids exert on the overall performance of SiC ceramics [7].

The intricate relationship between microstructural features and mechanical properties of porous SiC samples is clarified through detailed analysis. Substantial evidence indicates that sintering aid additives substantially modify microstructural characteristics, which in turn profoundly influence the mechanical behavior of materials. Additions of TiC, AlN, and B_4C have been used to refine grain boundary characteristics, increase density, and modify grain size. It is apparent from the micrographs that TiC incorporation leads to the reinforcement of the SiC matrix, resulting in increased toughness. This is likely due to the inherent toughness of TiC and its ability to deflect and hinder crack propagation. Furthermore, the presence of AlN

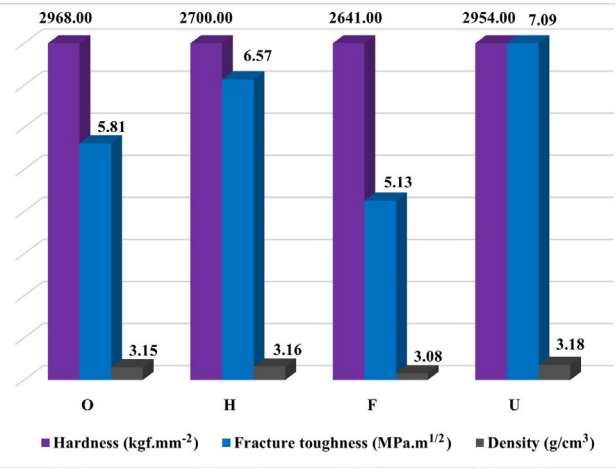

Fig. 6. The bending strengths, densities, and toughness values of as-SPSed samples.

appears to preserve the integrity of the cubic structure, likely due to its compatibility with the SiC matrix and its effective pinning of grain boundaries, which prevents excessive grain growth. This preservation is central to maintaining the material's innate strength [42]. Meanwhile, the inclusion of B_4C is associated with an increase in compressive strength, a phenomenon that may be attributed to the formation of a residual compressive stress field in the material as B_4C undergoes thermal expansion mismatch with the SiC matrix. These microstructural features improve load distribution in the composite, thereby reducing the risk of catastrophic failure. Hence, each additive uniquely influences the SiC microstructure, which in turn has a direct and calculable effect on the resultant mechanical properties such as strength, hardness, and toughness.

4. Conclusions

In this study, various sintering aids were employed to promote the mechanical properties (hardness, bending strength, compressive strength, fracture toughness) of silicon carbide. Four SiC-based samples including 2.5 wt% B_4C, 2.5 wt% AlN, and TiC ranging from 5 to 7 wt% were fabricated using the spark plasma sintering method at 1700 °C, with additives. The results indicate that incorporating 2.5 wt% AlN and 2.5 wt% B_4C increases the composite strength to 1206 MPa by creating compressive stress at the grain boundaries, though it reduces fracture toughness to 5.13 $MPa.m^{1/2}$. Conversely, the addition of TiC to SiC improves both toughness (7.09 $MPa.m^{1/2}$) and density (3.18 g/cm^3) compared to monolithic SiC.

CRediT authorship contribution statement

A. Faeghinia: Conceptualization, Investigation, Writing – original draft, Writing – review & editing.

Data availability

The data underlying this article will be shared on reasonable request to the corresponding author.

Declaration of competing interest

The authors declare no competing interests.

Funding and acknowledgment

The author gratefully acknowledges the generous support provided by the Materials and Energy Research Center.

References

[1] S. Sun, J. Yuan, W. Guo, X. Duan, D. Jia, H. Lin, Thickness effects on the sinterability, microstructure, and nanohardness of SiC-based ceramics consolidated by spark plasma sintering, J. Am. Ceram. Soc. 107 (2024) 777–784. https://doi.org/10.1111/jace.19499.

[2] S. Singh, R. Bhaskar, K.B. Narayanan, A. Kumar, K. Debnath, Development of silicon carbide (SiC)-based composites as microwave-absorbing materials (MAMs): a review, J. Eur. Ceram. Soc. (2024). https://doi.org/10.1016/j.jeurceramsoc.2024.05.032.

[3] J. Liu, Y. Li, C. Cheng, W. Li, X. Qin, Effect of temperature on the structure and mechanical properties of SiC–TiB2 composite ceramics by solid-phase spark plasma sintering, Ceram. Int. 48 (2022) 23151–23158. https://doi.org/10.1016/j.ceramint.2022.04.296.

[4] J. Shao, M. Li, K. Chang, Y. Huang, D. Ren, et al., Fabrication and characterization of SPS sintered SiC-based ceramic from Y3Si2C2-coated SiC powders, J. Eur. Ceram. Soc. 38 (2018) 4833–4841. https://doi.org/10.1016/j.jeurceramsoc.2018.07.054.

[5] E. Akbari, M. Ghassemi Kakroudi, V. Shahedifar, H. Ghiasi, The influence of different SiC amounts on the microstructure, densification, and mechanical properties of hot-pressed Al 2 O 3 - SiC composites, Int. J. Appl. Ceram. Technol. 17 (2020) 491–500. https://doi.org/10.1111/ijac.13406.

[6] Z. Zhang, C. Xu, X. Du, Z. Li, J. Wang, et al., Synthesis mechanism and mechanical properties of TiB2–SiC composites fabricated with the B4C–TiC–Si system by reactive hot pressing, J. Alloys Compd. 619 (2015) 26–30. https://doi.org/10.1016/j.jallcom.2014.09.030.

[7] D. Ahmoye, D. Bucevac, V.D. Krstic, Mechanical properties of reaction sintered SiC-TiC composite, Ceram. Int. 44 (2018) 14401–14407. https://doi.org/10.1016/j.ceramint.2018.05.050.

[8] S. Prochazka, R.M. Scanlan, Effect of boron and carbon on sintering of SiC, J. Am. Ceram. Soc. 58 (1975) 72–72. https://doi.org/10.1111/j.1151-2916.1975.tb18990.x.

[9] P. Sahani, S.K. Karak, B. Mishra, D. Chakravarty, D. Chaira, Effect of Al addition on SiC–B4C cermet prepared by pressureless sintering and spark plasma sintering methods, Int. J. Refract. Met. Hard Mater. 57 (2016) 31–41. https://doi.org/10.1016/j.ijrmhm.2016.02.005.

[10] M. khodaei, O. Yaghobizadeh, S.H. Naghavi Alhosseini, S. Esmaeeli, S.R. Mousavi, The effect of oxide, carbide, nitride and boride additives on properties of pressureless sintered SiC: A review, J. Eur. Ceram. Soc. 39 (2019) 2215–2231. https://doi.org/10.1016/j.jeurceramsoc.2019.02.042.

[11] J. Li, X. Ren, Y. Zhang, H. Hou, S. Hu, Rapid refinement of SiC particles by a novel milling process with balls of multiple sizes, J. Mater. Res. Technol. 9 (2020) 8667–8674. https://doi.org/10.1016/j.jmrt.2020.05.090.

[12] A. Zangvil, R. Ruh, Phase relationships in the silicon carbide-aluminum nitride system, J. Am. Ceram. Soc. 71 (1988) 884–890. https://doi.org/10.1111/j.1151-2916.1988.tb07541.x.

[13] G.H. Wroblewska, E. Nold, F. Thümmler, The role of boron and carbon additions on the microstructural development of pressureless sintered silicon carbide, Ceram. Int. 16 (1990) 201–209. https://doi.org/10.1016/0272-8842(90)90067-P.

[14] A. Maître, A. Vande Put, J.P. Laval, S. Valette, G. Trolliard, Role of boron on the spark plasma sintering of an α-SiC powder, J. Eur.

Ceram. Soc. 28 (2008) 1881–1890. https://doi.org/10.1016/j.jeurceramsoc.2008.01.002.
[15] N. Tamari, T. Tanaka, K. Tanaka, I. Kondoh, M. Kawahara, M. Tokita, Effect of spark plasma sintering on densification and mechanical properties of silicon carbide, J. Ceram. Soc. Japan. 103 (1995) 740–742. https://doi.org/10.2109/jcersj.103.740.
[16] Y. Zhou, K. Hirao, M. Toriyama, H. Tanaka, Very rapid densification of nanometer silicon carbide powder by pulse Electric current sintering, J. Am. Ceram. Soc. 83 (2000) 654–656. https://doi.org/10.1111/j.1151-2916.2000.tb01249.x.
[17] R.A. Alliegro, L.B. Coffin, J.R. Tinklepaugh, Pressure-sintered silicon carbide, J. Am. Ceram. Soc. 39 (1956) 386–389. https://doi.org/10.1111/j.1151-2916.1956.tb15609.x.
[18] D.H. Stutz, S. Prochazka, J. Lorenz, Sintering and microstructure formation of β-silicon carbide, J. Am. Ceram. Soc. 68 (1985) 479–482. https://doi.org/10.1111/j.1151-2916.1985.tb15812.x.
[19] M.S. Datta, A.K. Bandyopadhyay, B. Chaudhuri, Sintering of nano crystalline α silicon carbide by doping with boron carbide, Bull. Mater. Sci. 25 (2002) 181–189. https://doi.org/10.1007/BF02711151.
[20] A.G. Evans, E.A. Charles, Fracture toughness determinations by indentation, J. Am. Ceram. Soc. 59 (1976) 371–372. https://doi.org/10.1111/j.1151-2916.1976.tb10991.x.
[21] K. Raju, D.-H. Yoon, Sintering additives for SiC based on the reactivity: A review, Ceram. Int. 42 (2016) 17947–17962. https://doi.org/10.1016/j.ceramint.2016.09.022.
[22] A. Malinge, A. Coupé, Y. Le Petitcorps, R. Pailler, Pressureless sintering of beta silicon carbide nanoparticles, J. Eur. Ceram. Soc. 32 (2012) 4393–4400. https://doi.org/10.1016/j.jeurceramsoc.2012.06.008.
[23] D. Bucevac, S. Boskovic, B. Matovic, V. Krstic, Toughening of SiC matrix with in-situ created TiB2 particles, Ceram. Int. 36 (2010) 2181–2188. https://doi.org/10.1016/j.ceramint.2010.06.001.
[24] D. Jain, K.M. Reddy, A. Mukhopadhyay, B. Basu, Achieving uniform microstructure and superior mechanical properties in ultrafine grained TiB2–TiSi2 composites using innovative multi stage spark plasma sintering, Mater. Sci. Eng. A. 528 (2010) 200–207. https://doi.org/10.1016/j.msea.2010.09.022.
[25] W.J. MoberlyChan, J.J. Cao, C.J. Gilbert, R.O. Ritchie, L.C. De Jonghe, The cubic-to-hexagonal transformation to toughen SiC, Ceram. Microstruct., Springer US, Boston, MA. (1998) 177–190. https://doi.org/10.1007/978-1-4615-5393-9_15.
[26] A. Laref, S. Laref, Opto-electronic study of SiC polytypes: simulation with semi-empirical tight-binding approach, Silicon Carbide - Mater. Process. Appl. Electron. Devices, InTech. (2011). https://doi.org/10.5772/24124.
[27] S. Adachi, Hexagonal silicon carbide (2H-, 4H-, and 6H-SiC), Opt. Constants Cryst. Amorph. Semicond., Springer US, Boston, MA. (1999) 73–90. https://doi.org/10.1007/978-1-4615-5247-5_7.
[28] Z. Wang, F. Gao, N. Li, N. Qu, H. Gou, X. Hao, Density functional theory study of hexagonal carbon phases, J. Phys. Condens. Matter. 21 (2009) 235401. https://doi.org/10.1088/0953-8984/21/23/235401.
[29] C.S. Smith, Patent: Trans. AIME 175 (1948).
[30] J.B. Ferguson, H.F. Lopez, P.K. Rohatgi, K. Cho, C.-S. Kim, Impact of volume fraction and size of reinforcement particles on the grain size in metal–matrix micro and nanocomposites, Metall. Mater. Trans. A. 45 (2014) 4055–4061. https://doi.org/10.1007/s11661-014-2358-2.
[31] T. Tani, Processing, microstructure and properties of in-situ reinforced SiC matrix composites, Compos. Part A Appl. Sci. Manuf. 30 (1999) 419–423. https://doi.org/10.1016/S1359-835X(98)00129-8.
[32] W. Wang, J. Lian, H. Ru, Pressureless sintered SiC matrix toughened by in situ synthesized TiB2: Process conditions and fracture toughness, Ceram. Int. 38 (2012) 2079–2085. https://doi.org/10.1016/j.ceramint.2011.10.045.
[33] I. Sulima, P. Putyra, P. Hyjek, T. Tokarski, Effect of SPS parameters on densification and properties of steel matrix composites, Adv. Powder Technol. 26 (2015) 1152–1161. https://doi.org/10.1016/j.apt.2015.05.010.
[34] A. Kubiak, J. Rogowski, Boron and aluminum diffusion into 4H–SiC substrates, Mater. Sci. Eng. B. 176 (2011) 297–300. https://doi.org/10.1016/j.mseb.2010.06.022.
[35] W. Zhang, An overview of the synthesis of silicon carbide–boron carbide composite powders, Nanotechnol. Rev. 12 (2023) 20220571. https://doi.org/10.1515/ntrev-2022-0571.
[36] Y. Luo, S. Li, W. Pan, L. Li, Fabrication and mechanical evaluation of SiC–TiC nanocomposites by SPS, Mater. Lett. 58 (2004) 150–153. https://doi.org/10.1016/S0167-577X(03)00434-8.
[37] L. Liang, B. Wei, M. Zhang, W. Fang, L. Chen, Y. Wang, Novel TiC-based ceramic with enhanced mechanical properties by reaction hot-pressing at low temperature, J. Mater. Res. Technol. 24 (2023) 2129–2143. https://doi.org/10.1016/j.jmrt.2023.03.111.
[38] M. Yi, X. Zhang, G. Liu, B. Wang, H. Shao, G. Qiao, Comparative investigation on microstructures and mechanical properties of (TiB + TiC)/Ti-6Al-4V composites from Ti-B4C-C and Ti-TiB2-TiC systems, Mater. Charact. 140 (2018) 281–289. https://doi.org/10.1016/j.matchar.2018.04.010.
[39] Y. Cai, L. Cheng, H. Yin, X. Yin, Y. Tian, et al., Preparation and mechanical properties of Ti3SiC2/SiC functionally graded materials, Ceram. Int. 43 (2017) 6648–6658. https://doi.org/10.1016/j.ceramint.2017.02.025.
[40] M. Sakkaki, M. Foroutani, P. Zare, Effects of die geometry and insulation on the energy and electrical parameters analyses of spark plasma sintered TiC ceramics, Synth. Sinter. 4 (2024) 4–16. https://doi.org/10.53063/synsint.2024.41172.
[41] S. Mohammad Bagheri, M. Naderi, M. Vajdi, F. Sadegh Moghanlou, A. Tarlani Beris, Numerical optimization of sample and die geometric parameters to increase the attainable temperature during spark plasma sintering of TiC ceramics, Synth. Sinter. 3 (2023) 213–225. https://doi.org/10.53063/synsint.2023.34179.
[42] D.H.A. Besisa, E.M.M. Ewais, Y.M.Z. Ahmed, F.I. Elhosiny, T. Fend, D. V. Kuznetsov, Investigation of microstructure and mechanical strength of SiC/AlN composites processed under different sintering atmospheres, J. Alloys Compd. 756 (2018) 175–181. https://doi.org/10.1016/j.jallcom.2018.05.020.